Supplemental Materials

Source Apportionment of Soot Particles and Aqueous-Phase Processing of Black Carbon Coatings in an Urban Environment

Ryan N. Farley[1,2], Sonya Collier[1,a], Christopher D. Cappa[3], Leah R. Williams[4], Timothy B. Onasch[4], Lynn M. Russell[5], Hwajin Kim[1,b], Qi Zhang[1,2]

[1]Department of Environmental Toxicology, University of California Davis, CA, 95616, USA
[2]Agricultural and Environmental Chemistry Graduate Group, University of California Davis, CA 95616, USA
[3]Department of Civil and Environmental Engineering, University of California Davis, CA , 95616, USA
[4]Aerodyne Research Inc., Billerica, MA, 01821, USA
[5]Scripps Institution of Oceanography, University of California San Diego, CA, 92037, USA
[a]Now at: California Air Resources Board, 1001 I Street, Sacramento, CA 95814, USA
[b]Now at: Seoul National University, Seoul, South Korea

Correspondence to: Qi Zhang (dkwzhang@ucdavis.edu)

S1. Methods

S1.1 Sampling Site

The measurements were performed at the University of California Cooperative Extension, an urban site in Fresno, CA. The sampling location was surrounded by residential neighborhoods and a commercial center and was approximately 500m from a nearby highway. Instrumentation was housed in a temperature regulated trailer and ambient air was sampled at 1 m^3 min^{-1} from 6m above ground level. A flow of 10 L min^{-1} was subsampled and passed through a diffusion drier and $PM_{2.5}$ cyclone prior to a split between the real time instrumentation, including a soot-particle aerosol mass spectrometer (SP-AMS), high resolution aerosol mass spectrometer (HR-AMS), Cavity Ring Down Photoacoustic Spectrometer (CRD-PAS), Particle absorption eXtinctiometer (PAX), single particle soot photometer (SP2) and scanning mobility particle sizer (SMPS). Meteorology, including wind speed, wind direction, temperature and relative humidity was measured using a Vaisala WXT520 weather transmitter. Trace gas measurements including NO and NO_2 (T200 M, Teledyne API), CO (T300, Teledyne API) were also measured at the field site.

S1.2 Aerosol Optical Measurements and Absorption Enhancement Calculations

Optical properties were measured at 405 and 532nm using the University of California Davis dual wavelength cavity ringdown/photoacoustic spectrometer (CRD-PAS) and at 870nm using a photoacoustic eXtinctiometer (PAX; DMT Inc.) (Cappa et al., 2019; Langridge et al., 2011).

The absorption enhancement (E_{abs}) of black carbon due to the lensing effect was calculated based on the mass absorption coefficient (MAC_{BC}), and is detailed in (Cappa et al., 2019). Specifically, MAC_{BC} was calculated as:

$$MAC_{BC} = \frac{b_{abs}}{[BC]} \qquad (S1)$$

Where b_{abs} is the measured absorption and [BC] is the black carbon mass. Following this, the absorption enhancement was calculated as:

$$E_{abs} = \frac{MAC_{BC}}{MAC_{BC,ref}} \qquad (S2)$$

Where the $MAC_{BC,ref}$ was determined as the MAC for pure, uncoated BC. $MAC_{BC,ref}$ values used for this campaign were 4.4 ± 0.2 m^2 g^{-1} (870 nm), 7.5 ± 0.5 m^2 g^{-1} (532 nm), 10.7 ± 0.6 m^2 g^{-1} (405 nm). This enhancement accounts for both the absorption due to coating material (i.e. BrC) and the lensing effect. Because of this, all analysis regarding E_{abs} was done at 870 nm to reduce the overall influence of BrC.

S1.3 ME-2 Analysis

45   The SP-AMS matrix was prepared for PMF analysis following previously established guidelines (Ulbrich et al., 2009; Zhang et al., 2011). Noisy ions with signal-to-noise ratio (S/N) < 0.2 were removed and S/N < 2 were down-weighted. Ions scaled to CO_2^+ (i.e., O^+, OH^+, H_2O^+, CO^+) were removed and recalculated following the analysis (Canonaco et al., 2013).

    Initially, all solutions were allowed to vary freely, however it became evident that there was significant mixing between the hydrocarbon-like OA (HOA_{BC}) and biomass burning organic aerosol ($BBOA_{BC}$) factors. This was likely due to

50 the proximity of combustion sources and similar patterns of emissions, leading to strong temporal correlations between the two factors. To correct for this, the $BBOA_{BC}$ and HOA_{BC} spectra were constrained using the *a*-value approach within the SoFi software (Canonaco et al., 2013). With this method, *a priori* spectra are provided by the user and the solution is allowed to vary based on a preselected *a*-value, ranging between 0 (fully constrained) and 1 (unconstrained). The $BBOA_{BC}$ anchor spectrum selected for this study was the profile resolved in the 4-factor unconstrained analysis. If the number of factors was

55 increased beyond four during the unconstrained PMF analysis, splitting of the BBOA factor was seen. For the HOA_{BC} anchor spectrum, the HOA_{BC} spectrum resolved in the 5-factor unconstrained analysis was modified to remove the influence from BBOA. The 5-factor HOA_{BC} spectrum was selected as it had a smaller contribution from fragments associated with BBOA, such as $C_2H_4O_2^+$, compared to the 4-factor solution. The spectrum was further modified by subtracting a portion of each ion signal based on its ratio to the $C_2H_4O_2^+$ ion in the $BBOA_{BC}$ spectrum until the f_{60} reached the established background value of

60 0.3% (Cubison et al., 2011). BC and other inorganic fragments were included in the anchor spectra, however the intensity of these ions in the HOA_{BC} anchor spectrum were not modified.

    The 1 to 8 factor solutions were explored with *a*-values ranging from 0-0.8 for the $BBOA_{BC}$ and HOA_{BC} factors while the remaining factors were allowed to vary freely. A 4-factor solution with *a*-values of 0.4 for $BBOA_{BC}$ and HOA_{BC} was selected as the final solution. The spectra of the 3- and 5-factor solutions and the diagnostic plots are shown in Fig. S1-3. The

65 4-factor solution showed lower Q/Q_{exp} and improved residual over the 3-factor solution as a second OOA_{BC} factor was resolved (Fig. S3). However, moving from 4 to 5 factors resulted in further splitting of the OOA_{BC} factors with minimal additional chemical information. As the *a*-value was increased within the 4-factor solution, the $BBOA_{BC}$ factor remained similar, however the HOA_{BC} spectrum began to show signs of increasing BBOA "contamination". An *a*-value of 0.4 was selected as there was minimal improvement of Q/Q_{exp} at larger values and mixing of $BBOA_{BC}$ and HOA_{BC} remained minimized (Fig. S6b).

70 Furthermore, previous studies have also found that *a*-values of 0.4 are optimum (Canonaco et al., 2020; Sun et al., 2022). Despite this, we note that there is a slightly elevated f_{60} (0.45%) within the HOA_{BC} mass spectrum, suggesting a minor BBOA influence. Finally, the rotational ambiguity of the solution was explored by varying the fpeak value from -1 to 1. Minimal change was seen with varying fpeak and a value of 0 was chosen.

S1.4 Thermodynamic modeling

Aerosol liquid water content associated with rBC (ALWC$_{BC}$) was estimated using the Extended Aerosol Inorganic Model (E-AIM) using model II (http://www.aim.env.uea.ac.uk/aim/aim.php) (Clegg et al., 1998). This model uses the concentrations of NH_4^+, NO_3^- and SO_4^{2-} measured by the SP-AMS as well as the ambient temperature and relative humidity. As no $NH_{3(g)}$ measurements were collected, the model was run in reverse mode. The E-AIM model requires neutralized particles, therefore the charges were balanced using H^+ and OH^- as needed. E-AIM is not able to calculate the ALWC associated with organics (ALWC$_{Org}$), which previous research has been found to be non-negligible (Nguyen et al., 2016; Parworth et al., 2017). Instead ALWC$_{Org, rBC}$ was found using the following equation derived from (Petters and Kreidenweis, 2007):

$$ALWC_{Org,rBC} = \frac{m_{Org}\, \rho_w}{\rho_{Org}} \frac{\kappa_{Org}}{\left(\frac{1}{RH}-1\right)} \tag{S3}$$

Where m_{Org} is the measured OA mass from the SP-AMS, ρ_w is the density of water (1 g cm^{-3}), ρ_{Org} is the OA density, κ_{org} is the OA hygroscopicity parameter and RH is the measured relative humidity. ρ_{Org} was estimated based on the elemental composition with the following formula: $\rho_{Org} = [(12 + H/C) + 16*(O/C) / 7 + 5*(H/C) + 4.15*(O/C)]$ (Kuwata et al., 2012). As there were no direct measurements of the hygroscopicity of the black carbon containing aerosols, κ_{org} was parameterized using the SP-AMS f_{44} with the following relationship

$$\kappa_{Org} = 2.2 * f_{44} - 0.13 \tag{S4}$$

as described in (Duplissy et al., 2011). The total ALWC$_{rBC}$ is assumed to be the sum of ALWC$_{E-AIM,rBC}$ and ALWC$_{Org,rBC}$ and the time series of each is shown in Fig. S14.

References

Canonaco, F., Crippa, M., Slowik, J. G., Baltensperger, U. and Prévôt, A. S. H.: SoFi, an IGOR-based interface for the efficient use of the generalized multilinear engine (ME-2) for the source apportionment: ME-2 application to aerosol mass spectrometer data, Atmos. Meas. Tech., doi:10.5194/amt-6-3649-2013, 2013.

Canonaco, F., Tobler, A., Chen, G., Sosedova, Y., Slowik, J. G., Daellenbach, K. R., Elhaddad, I., Crippa, M., Huang, R., Baltensperger, U., Stephan, A. and Prévôt, H.: A new method for long-term source apportionment with time- dependent factor profiles and uncertainty assessment using SoFi Pro : application to one year of organic aerosol data, Atmos. Meas. Tech., (July), 1–39, 2020.

Cappa, C. D., Zhang, X., Russell, L. M., Collier, S., Lee, A. K. Y., Chen, C. L., Betha, R., Chen, S., Liu, J., Price, D. J., Sanchez, K. J., McMeeking, G. R., Williams, L. R., Onasch, T. B., Worsnop, D. R., Abbatt, J. and Zhang, Q.: Light Absorption by Ambient Black and Brown Carbon and its Dependence on Black Carbon Coating State for Two California, USA, Cities in Winter and Summer, J. Geophys. Res. Atmos., 124(3), 1550–1577, doi:10.1029/2018JD029501, 2019.

Clegg, S. L., Brimblecombe, P. and Wexler, A. S.: Thermodynamic model of the system H+-NH4+-SO42-NO 3--H2O at

tropospheric temperatures, J. Phys. Chem. A, 102(12), 2137–2154, doi:10.1021/jp973042r, 1998.

Cubison, M. J., Ortega, A. M., Hayes, P. L., Farmer, D. K., Day, D., Lechner, M. J., Brune, W. H., Apel, E., Diskin, G. S., Fisher, J. A., Fuelberg, H. E., Hecobian, A., Knapp, D. J., Mikoviny, T., Riemer, D., Sachse, G. W., Sessions, W., Weber, R. J., Weinheimer, A. J., Wisthaler, A. and Jimenez, J. L.: Effects of aging on organic aerosol from open biomass burning smoke in aircraft and laboratory studies, Atmos. Chem. Phys., doi:10.5194/acp-11-12049-2011, 2011.

Duplissy, J., Decarlo, P. F., Dommen, J., Alfarra, M. R., Metzger, A., Barmpadimos, I. and Prevot, A. S. H.: Relating hygroscopicity and composition of organic aerosol particulate matter, Atmos. Chem. Phys., 1155–1165, doi:10.5194/acp-11-1155-2011, 2011.

Kuwata, M., Zorn, S. R. and Martin, S. T.: Using elemental ratios to predict the density of organic material composed of carbon, hydrogen, and oxygen, Environ. Sci. Technol., 46(2), 787–794, doi:10.1021/es202525q, 2012.

Langridge, J. M., Richardson, M. S., Lack, D., Law, D. and Murphy, D. M.: Aircraft instrument for comprehensive characterization of aerosol optical properties, part i: Wavelength-dependent optical extinction and its relative humidity dependence measured using cavity ringdown spectroscopy, Aerosol Sci. Technol., 45(11), 1305–1318, doi:10.1080/02786826.2011.592745, 2011.

Nguyen, T. K. V, Zhang, Q., Jimenez, J. L., Pike, M. and Carlton, A. G.: Liquid Water : Ubiquitous Contributor to Aerosol Mass, , doi:10.1021/acs.estlett.6b00167, 2016.

Parworth, C., Young, D. E., Kim, H., Zhang, X., Cappa, C. D., Collier, S. and Zhang, Q.: Wintertime water-soluble aerosol composition and particle water content in Fresno, California, J. Geophys. Res. Atmos., 122, 3155–3170, doi:10.1002/2016JD026173, 2017.

Petters, M. D. and Kreidenweis, S. M.: A single parameter representation of hygroscopic growth and cloud condensation nucleus activity, Atmos. Chem. Phys., 13(2), 1081–1091, doi:10.5194/acp-13-1081-2013, 2007.

Sun, P., Farley, R. N., Li, L., Srivastava, D., Niedek, C. R., Li, J., Wang, N., Cappa, C. D., Pusede, S. E., Yu, Z., Croteau, P. and Zhang, Q.: PM2.5 composition and sources in the San Joaquin Valley of California : A long-term study using ToF-ACSM with the capture vaporizer, Environ. Pollut., 292(PA), 118254, doi:10.1016/j.envpol.2021.118254, 2022.

Ulbrich, I. M., Canagaratna, M. R., Zhang, Q., Worsnop, D. R. and Jimenez, J. L.: Interpretation of organic components from Positive Matrix Factorization of aerosol mass spectrometric data, Atmos. Chem. Phys., doi:10.5194/acp-9-2891-2009, 2009.

Zhang, Q., Jimenez, J. L., Canagaratna, M. R., Ulbrich, I. M., Ng, N. L., Worsnop, D. R. and Sun, Y.: Understanding atmospheric organic aerosols via factor analysis of aerosol mass spectrometry: A review, Anal. Bioanal. Chem., doi:10.1007/s00216-011-5355-y, 2011.

2. Supplemental Figures
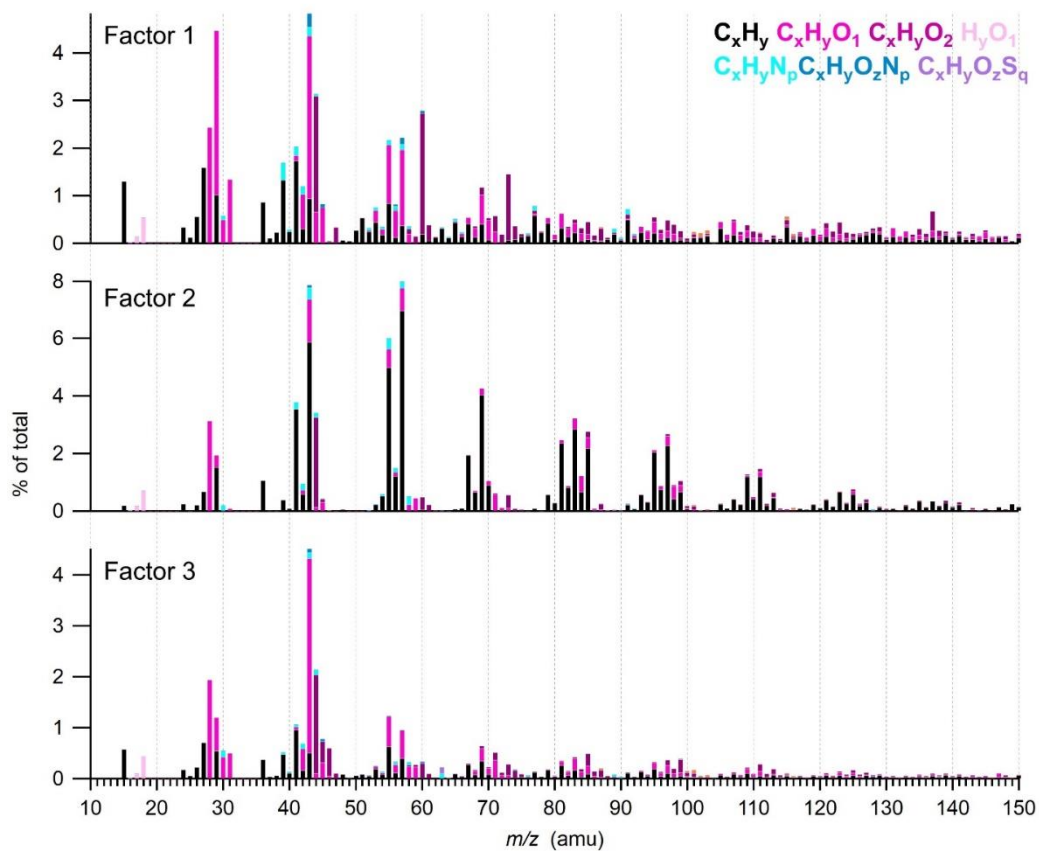
140

Figure S1: OA$_{BC}$ spectra for three factor PMF solution. Factor 1 is constrained to BBOA and factor 2 is constrained to HOA with a values of 0.4.
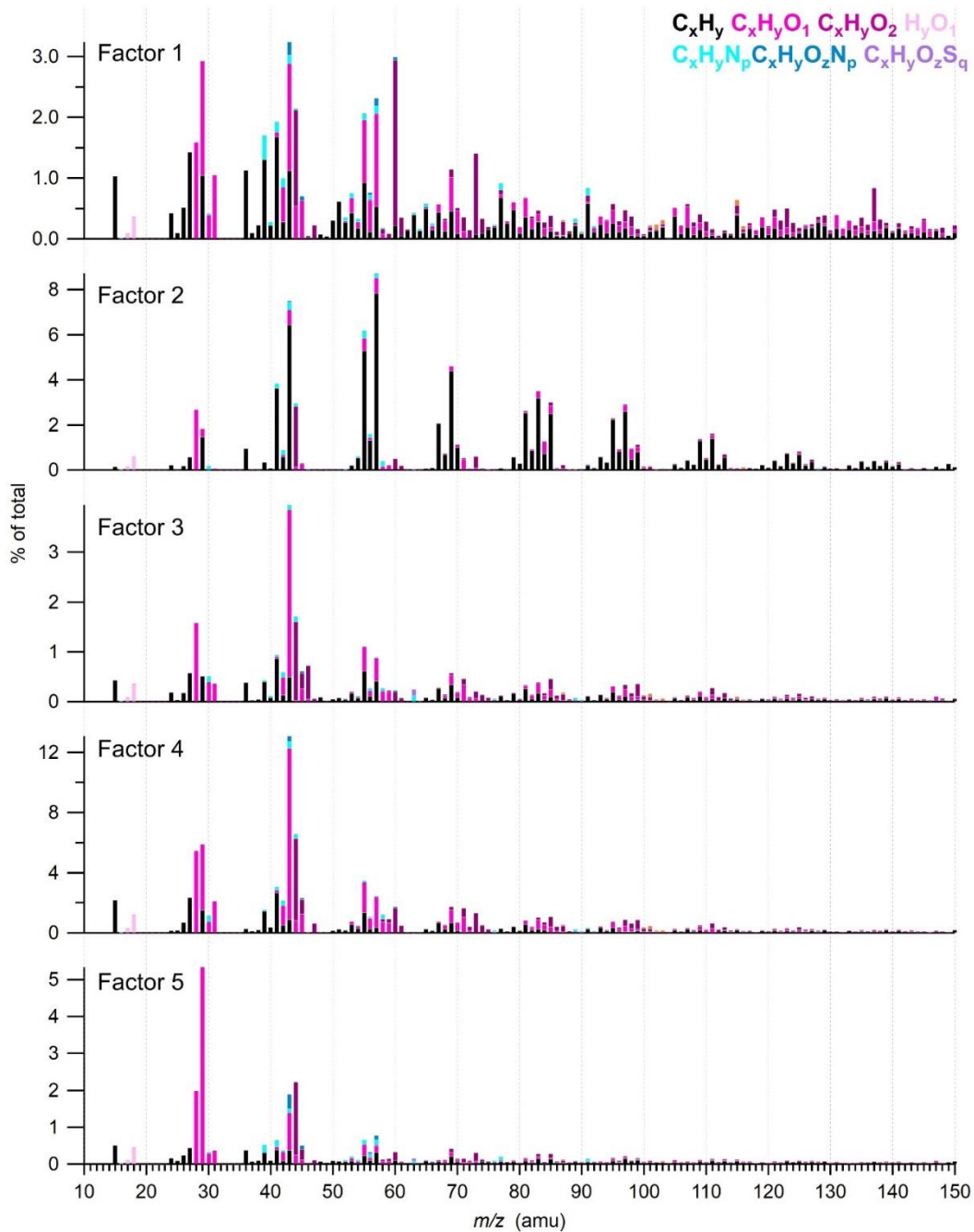
Figure S2: OABC spectra for five factor PMF solution. Factor 1 is constrained to BBOA and factor 2 is constrained to HOA with a values of 0.4.
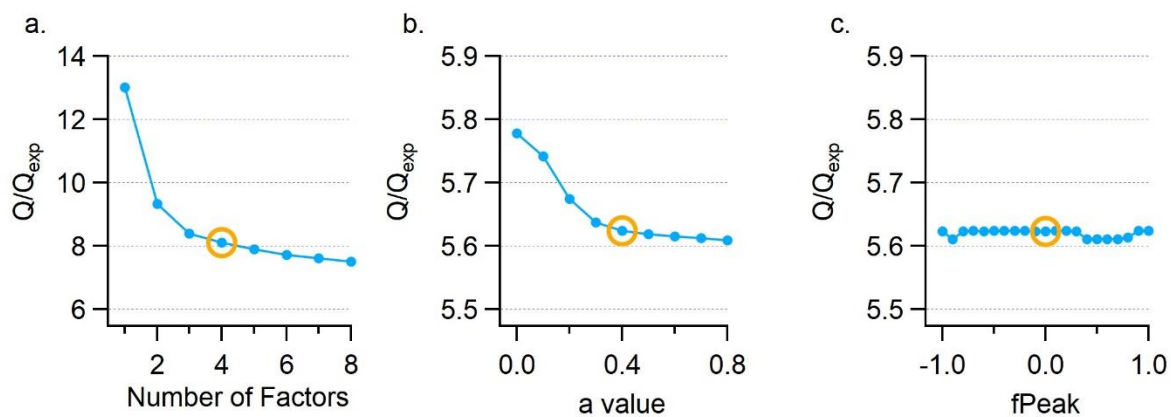
Figure S3: Change in Q/Qexp of PMF solution as function of (a) number of factors, (b) a-value, (c) fPeak. Values used in (a) are from the a-value of 0 and fPeak of 0. Values in (b) are for four factor solution and fPeak of 0. Values of (c) are for four factor solution and a-value of 0.4.

150
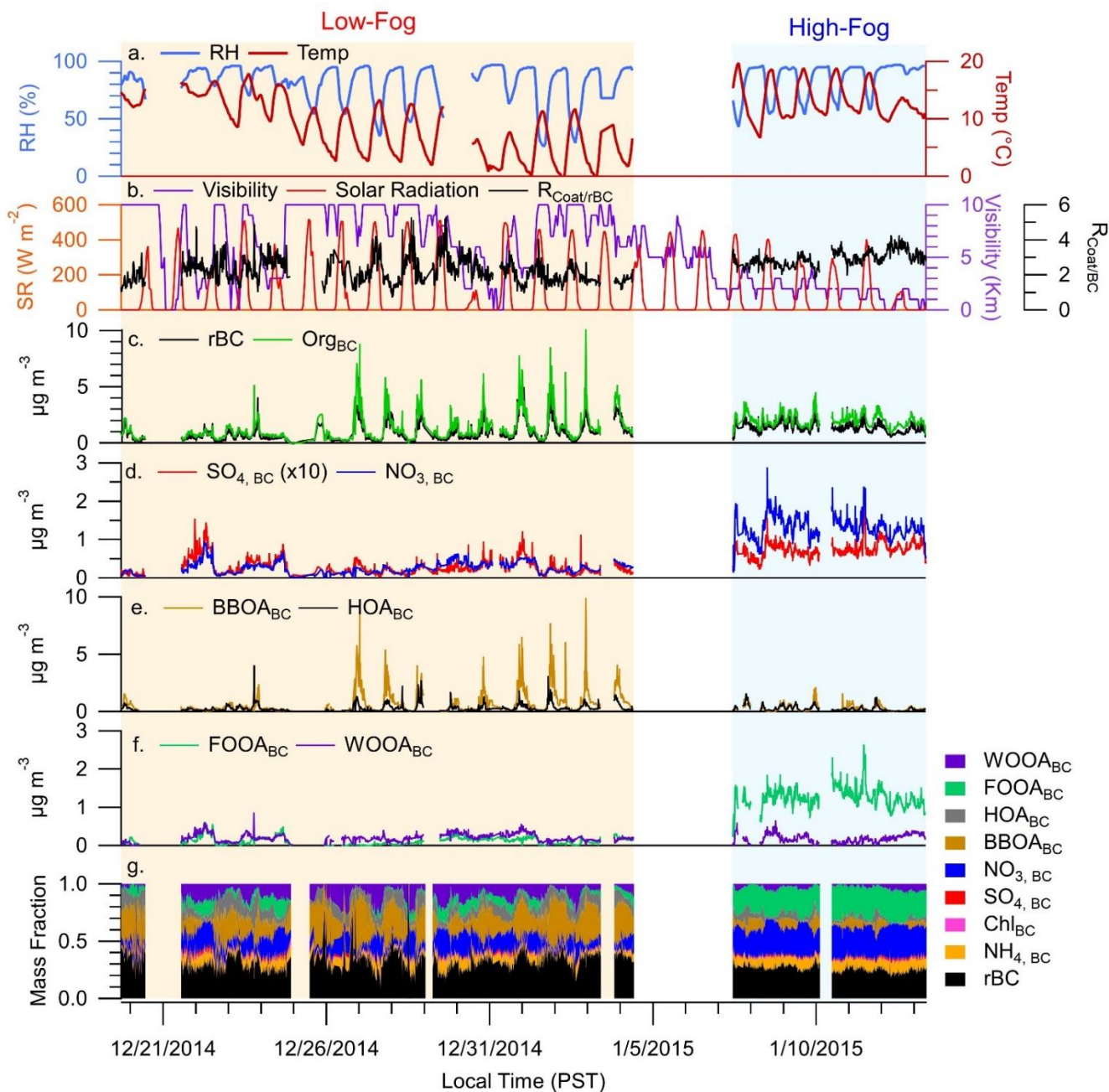
Figure S4: Time series of (a, b) meteorological parameters (b) bulk rBC coating thickness (c, d) PM1,BC species, (e,f) OABC factors resolved with PMF and (g) fractional contribution of each species to total PM1,BC. The blue background represents the fog case study period, while the orange background represents the contrasting low fog period. Gaps indicate missing data.
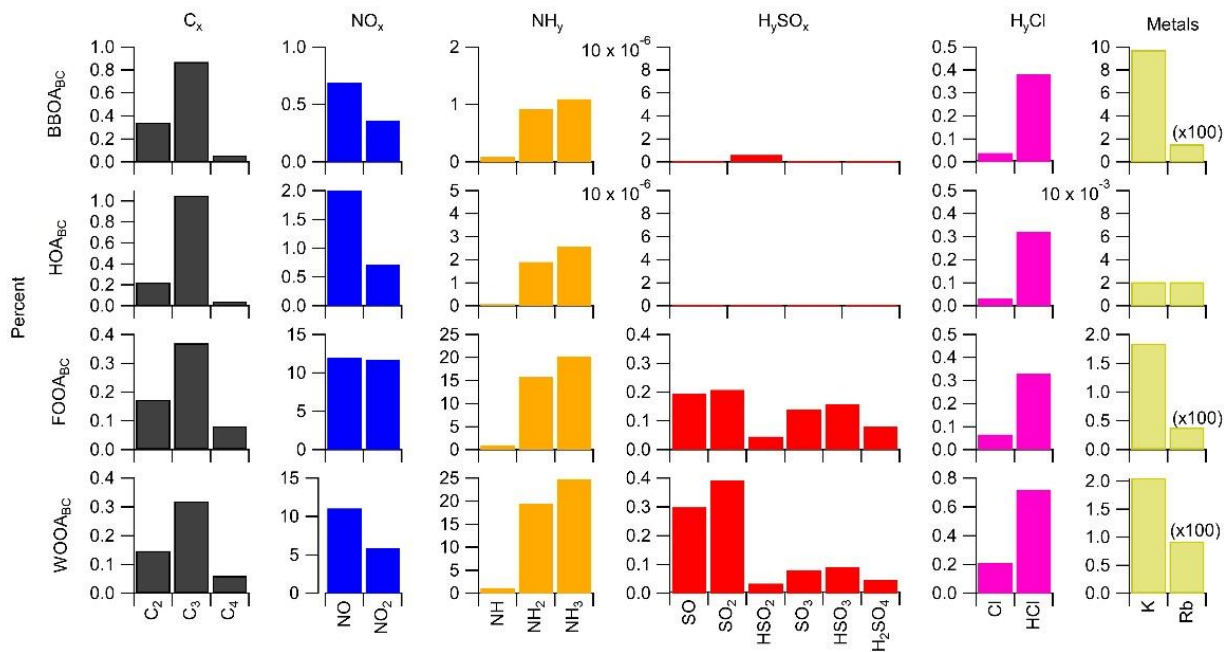
Figure S5: Distribution of inorganic ions across PMF factors, separated by chemical species. Axis values are percent of total nitrate equivalent signal.

160
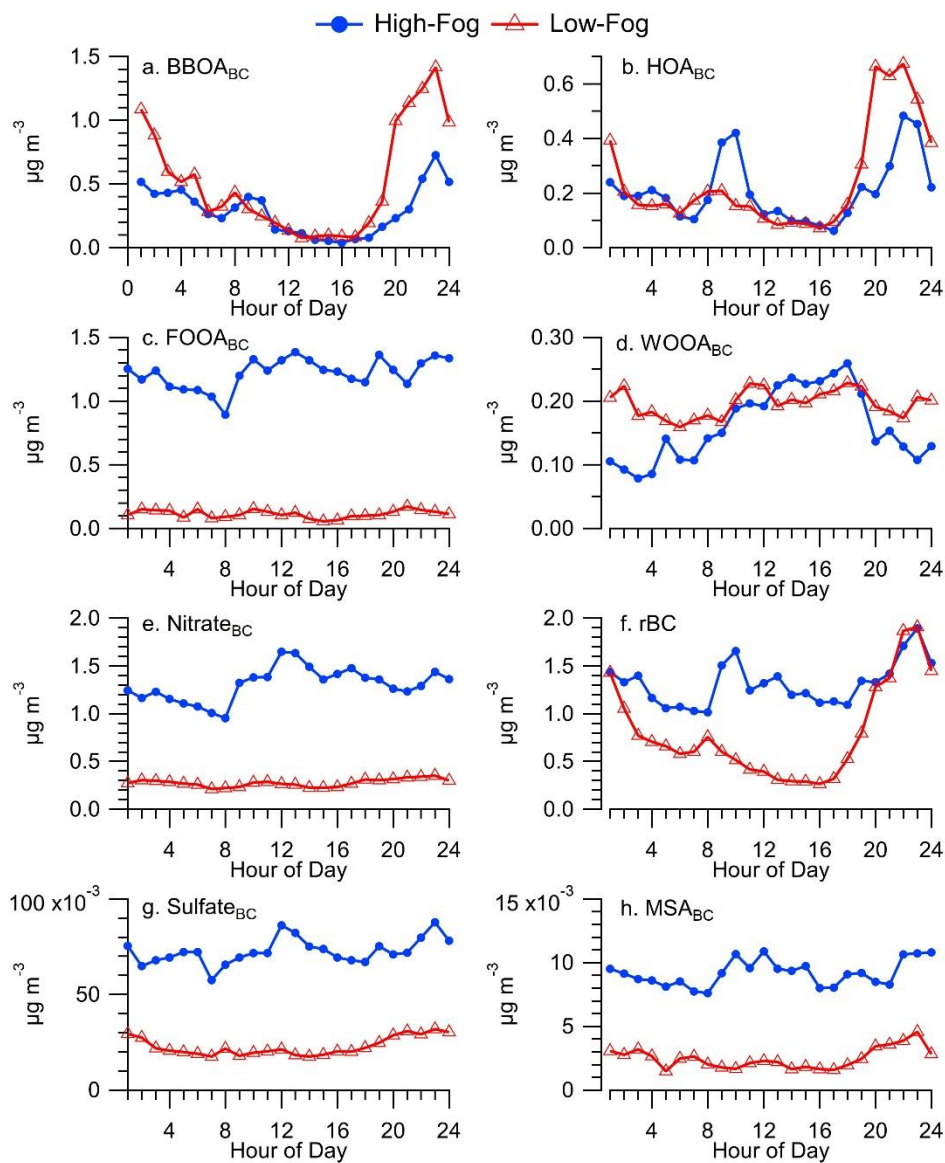
Figure S6: Diurnal profiles of hourly median concentration of (a) BBOA_BC, (b) HOA_BC, (c) FOOA_BC, (d) WOOA_BC, (e) Nitrate_BC, (f) rBC, (g) Sulfate_BC, (h) estimated MSA_BC. Concentration of each species is separated between the high-fog period and low-fog periods.

165
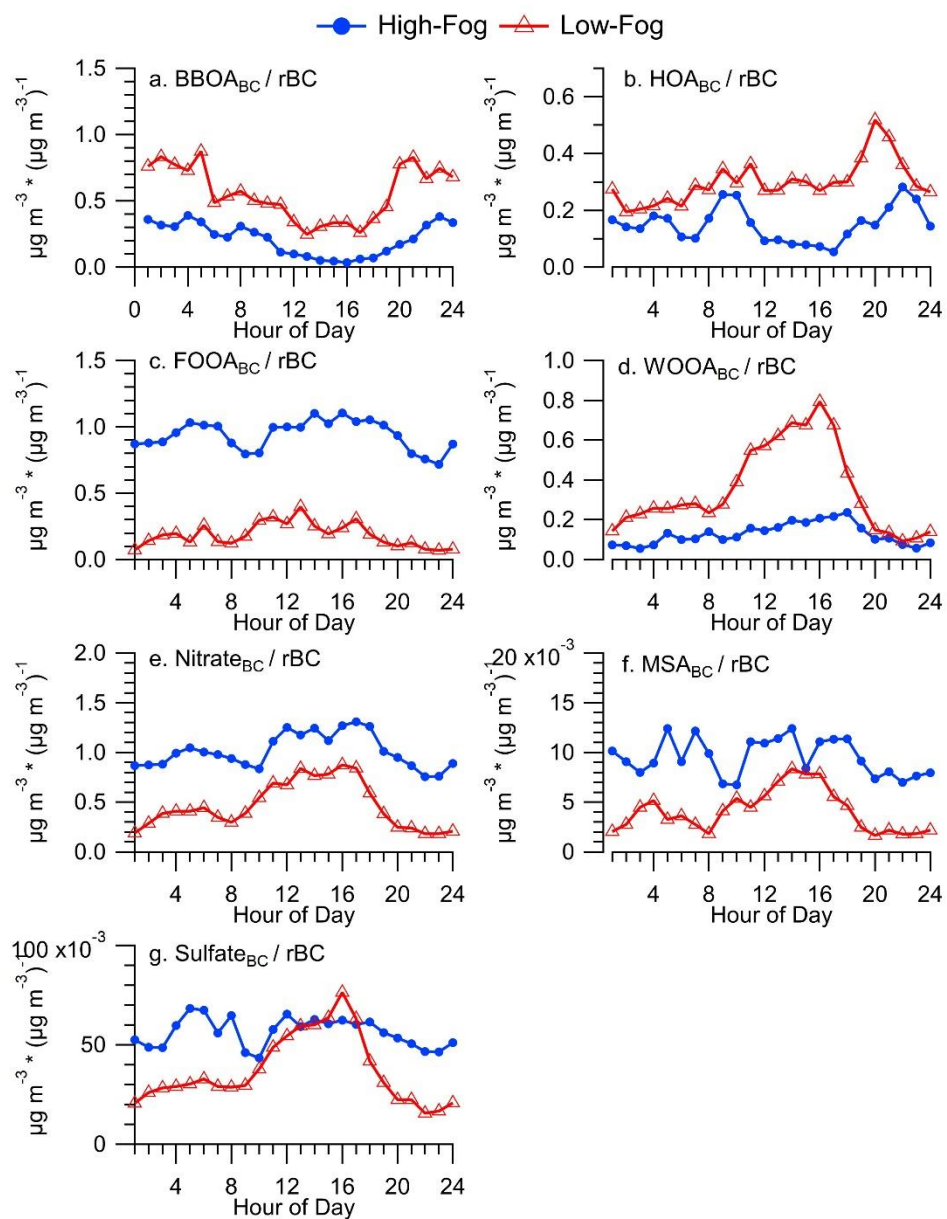
Figure S7: Same as Figure S6, however concentration is normalized by rBC concentration.
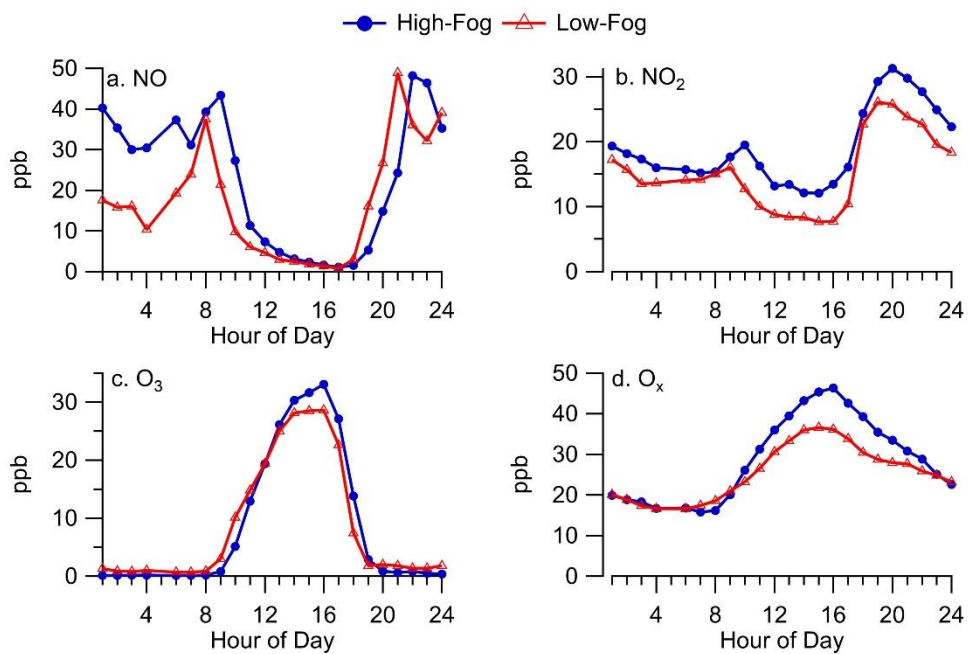
170   **Figure S8: Diurnal profile of gas-phase species (a) NO, (b) NO_2, (c) O_3 and (d) O_x. O_x equals the sum of O_3 and NO_2.**
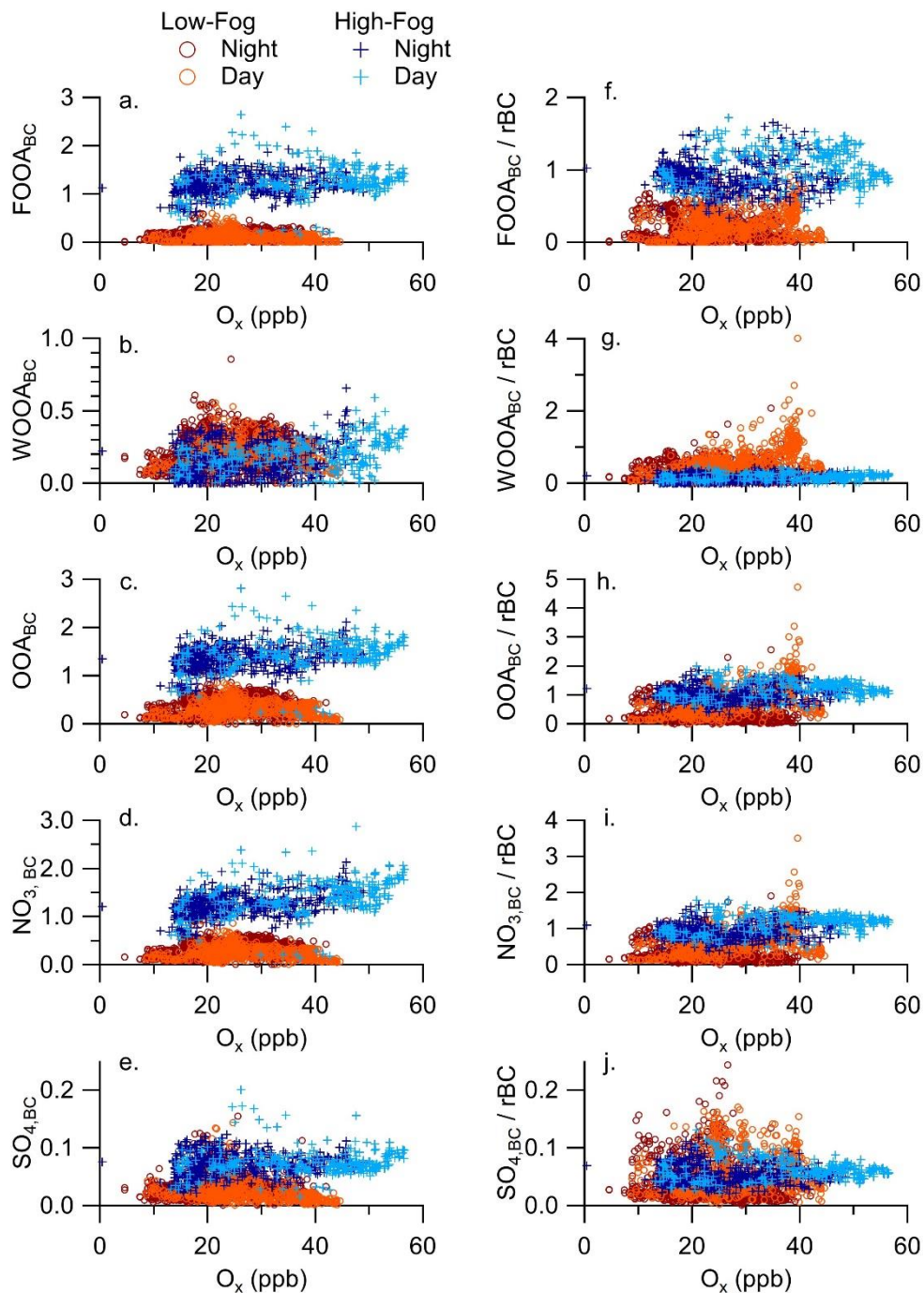
Figure S9: Relationship between (a) FOOA$_{BC}$, (b) WOOA$_{BC}$, (c) sum of FOOA$_{BC}$ and WOOA$_{BC}$, (d) NO$_{3,BC}$, (e) SO$_{4,BC}$ and O$_x$. (f-j) Same as (a-e) except concentration is normalized by rBC concentration. Data is separated between the fog period and low fog period as well as between day and night.
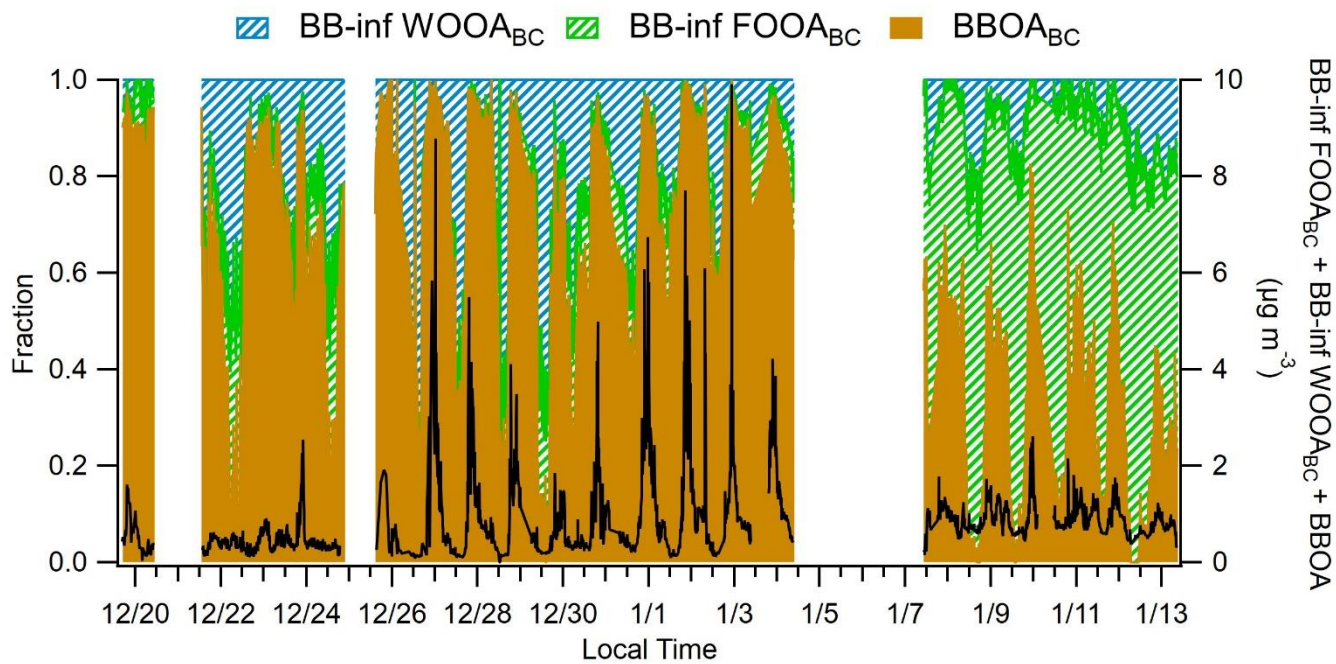
Figure S10: **Fractional contribution of BB-influenced WOOA, BB-influenced FOOA and BBOA. Black trace is the sum of the three species.**
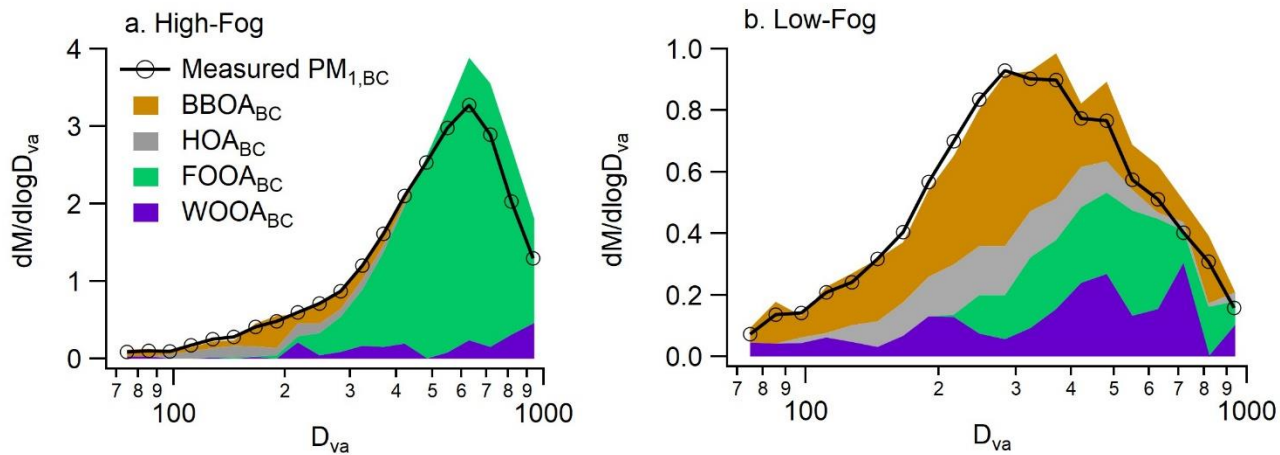
Figure S11: Comparison of SP-AMS measured PM$_{1,BC}$ size distribution (black line) and results of the linear decomposition of the size resolved mass spectra for the (a) fog period and (b) low fog period. Top panels show the scaled residual between the measured and modeled size distributions.
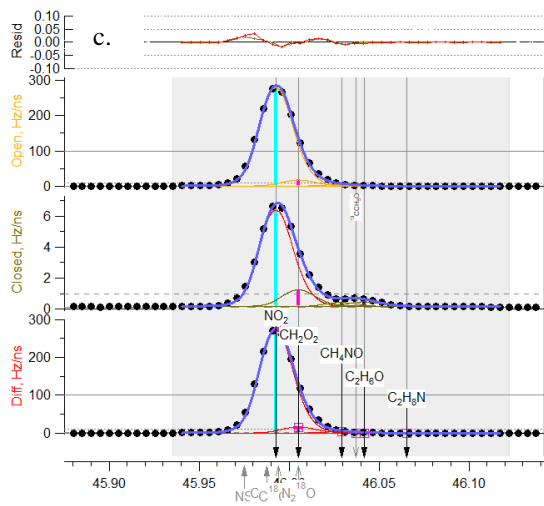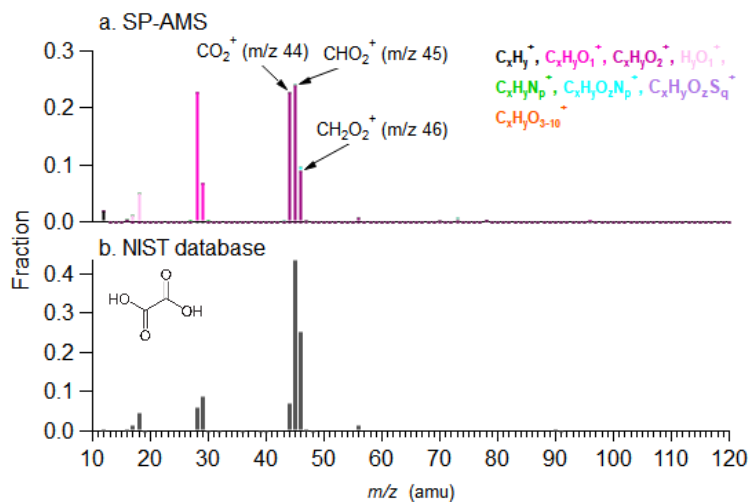
Figure S13: (a) SP-AMS mass spectrum of pure oxalic acid sampled in the laboratory. (b) Reference mass spectrum for oxalic acid from the NIST databases. (c) High resolution peak fitting of m/z 46 during a representative section of the fog period.
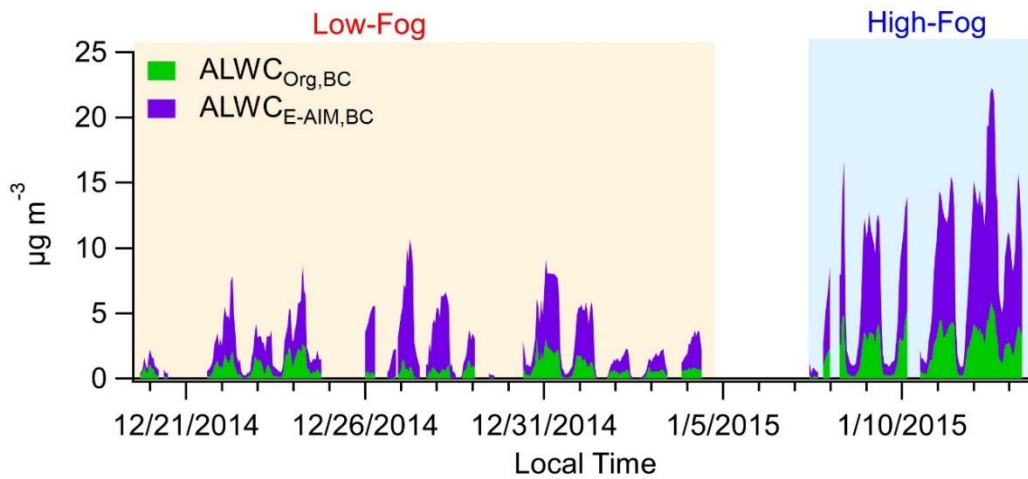
Figure S14: Stacked time series of ALWC_BC associated with inorganics calculating using E-AIM (ALWC_{E-AIM,BC}) and ALWC_BC associated with organics (ALWC_{Org,BC}).